THE UNIVERSITY OF WARWICK

Original citation:
Zafari, Behrouz and Mottram, J. Toby (James Toby), 1958-. (2014) Characterization by full-size testing of pultruded frame joints for the Startlink house. Journal of Composites in Construction . pp. 1-9. ISSN 1090-0268

Permanent WRAP url:
http://wrap.warwick.ac.uk/63289

Copyright and reuse:
The Warwick Research Archive Portal (WRAP) makes this work by researchers of the University of Warwick available open access under the following conditions. Copyright © and all moral rights to the version of the paper presented here belong to the individual author(s) and/or other copyright owners. To the extent reasonable and practicable the material made available in WRAP has been checked for eligibility before being made available.

Copies of full items can be used for personal research or study, educational, or not-for profit purposes without prior permission or charge. Provided that the authors, title and full bibliographic details are credited, a hyperlink and/or URL is given for the original metadata page and the content is not changed in any way.

Publisher's statement:
Published version: http://dx.doi.org/10.1061/(ASCE)CC.1943-5614.0000488

A note on versions:
The version presented here may differ from the published version or, version of record, if you wish to cite this item you are advised to consult the publisher's version. Please see the 'permanent WRAP url' above for details on accessing the published version and note that access may require a subscription.

For more information, please contact the WRAP Team at: publications@warwick.ac.uk

warwickpublicationswrap

highlight your research

http://wrap.warwick.ac.uk

Zafari and J. T. MOTTRAM, 'Characterization by full-size testing of pultruded frame joints for the Startlink house,' *Journal of Composites for Construction*, 2014, pp. 10. ISSN 1090-0268 http://ascelibrary.org/doi/abs/10.1061/(ASCE)CC.1943-5614.0000488?af=R&

Characterization by Full-size Testing of Pultruded Frame Joints for the Startlink House

B. Zafari[1] and J. T. Mottram[2]

Abstract: Presented in this paper are test results to determine the moment-rotation characteristics of joint details for a portal frame specific to a pultruded fiber reinforced polymer assembly for the Startlink house. Two joints having beam-to-column dowel connections, with and without extra adhesively bonding, were statically loaded in increments of moment or rotation to ultimate failure. The floor beam and stud column members are bespoke closed-sections developed for the Startlink lightweight building system. The serviceability design calculations for the demonstrator house to be constructed in Bourne, England, assumed the frame's joints to be rigid. Clauses in EN 1993-1-8:2005 have been applied to classify the measured rotational stiffnesses against the rigid requirement, and an evaluation is made of the modes of failure with respect to the joint's design moments. Only the joint with extra bonding between the mating surfaces of members is found to be classified as rigid. Both joints are shown to have an acceptable joint strength.

Keywords: Pultruded shapes, portal frame joints, doweled connections, Startlink house

1. Research Fellow, Civil Research Group, School of Engineering, The University of Warwick, CV4 7AL, UK. E-mail: B.Zafari@warwick.ac.uk

2. Professor, Civil Research Group, School of Engineering, The University of Warwick, CV4 7AL, UK. E-mail: J.T.Mottram@warwick.ac.uk

Introduction

In June 2008 the Technology Strategy Board, UK, announced investment in an R&D project to transform the Startlink Lightweight Building System (SLBS) from a concept into reality (Singleton and Hutchinson 2007; Hutchinson and Hartley 2011). The UK construction market is worth over £100 billion per year, and there is growing pressure from customers and regulators for more environmentally efficient buildings. The SLBS is an engineered solution from a consortium of six UK companies, led by EXEL Composites UK, together with academic structural engineering support from The University of Warwick. The goal was to produce a family of pultruded Fibre Reinforced Polymer (FRP) shapes (Bank 2006) that can be assembled, off-site, into panels for the house's superstructure. By integrating an energy management scheme this innovative house unit has the potential to satisfy the UK Government's requirement for Code Level 6 (Anonymous 2007). Legalisation from 2016 is requiring all new-built residential units in the UK to be carbon neutral over their working life. The innovative SLBS approach has been designed specifically to meet this demanding challenge using only composite material components.

To be able to engineer the Startlink house's superstructure required: knowledge of mechanical properties; working out how the frame members will connect together; establishing the stiffness of the whole frame system. The purpose of this paper is to report results from a fact finding test series on two full-sized single-sided beam-to-column joints. In Figure 1 are shown schematically the portal frame (not to scale) for the house unit with three floors (one at roof level), and the SPJ test specimen (with dimensions) for an external frame joint at the first floor level. The choice of letters in a specimen's abbreviation SPJ are: 'S' for Startlink, 'P' for Portal frame and 'J' for Joint.

The objective of the testing was to evaluate the performance of the frame joint in terms of rotational stiffness and strength (joint moment). Based on the design of the portal frame in Figure 1 the lateral stiffness was generated from assuming all joints are rigid. Because no practical joint detailing will be fully rigid, the moment-rotation (M-ϕ) characteristics (to failure) were required to establish what detailing was to be executed when the demonstrator house was constructed during 2012.

Figure 2 shows how the superstructure is assembled with a frame unit spaced every 0.6 m. The current design for the Startlink house has a structural system with no vertical bracing in the form of diagonal members. Given that the structural system does not possess bracing members, and there was no knowledge on the racking stiffness from the inner and outer wall panels, the house was designed by assuming that rigid frame action opposes the lateral (wind) loading.

For a rigid frame the moments, shear forces and axial forces at the joints were determined under design load cases due to combinations of live and dead vertical loading, and lateral wind loading. There is not space herein to present this background design work carried out by D. Kendall of Optima Projects Ltd., UK. Wind loading on outer walls was determined in accordance with BS 6399-2:1997 (British Standards Institution 1997). The partial load factor (γ_f) was in accordance with the EUROCOMP design publication (Clarke 1996). To obtain the Ultimate Limit State (ULS) loading a γ_f of 1.5 was applied to the Serviceability Limit State (SLS design) loading. The deflection limit under SLS loading for floor spans is span/480 and floor height is height/300. These vertical and horizontal SLS design limits were taken from timber design practice. The latter lateral deflection limit is the one that governs structural design of the frame.

It is worthy of mention that the test results for the two joints are taken from a series of four Sub-Assembly Joints (SAJ) tests that are presented in Chapter 6 of the PhD thesis by Zafari (2013). Convenience is the reason why the two joint specimens in this paper have be given labels SPJ-1 and SPJ-2. Justification for the specimen choice is that one joint (SPJ-1) is a pragmatic choice for buildability and rigid stiffness, and the second joint (SPJ-2) bests satisfy the design and build specifications for achieving the stiffest joint with dowel connections.

BS EN 1993-1-8:2005 (British Standards Institution 2005) has clauses for the stiffness and strength classifications of steel joints. This standard states that joint details should fulfil the assumptions made in the relevant design method (i.e. pinned (M = 0) or rigid (ϕ = 0)), without adversely affecting any other part of the structure. By assuming that the classification process is independent of material the Eurocode 3 procedure can be used to classify the FRP joints. For the design of the Startlink portal frame in Figures 1 and 2 the dominant criterion is joint rotational stiffness.

In what follows the authors provide information on materials and details of the tested joints, the methodology used to assemble them, the test rig and test procedure. Moment-rotation (M-ϕ) curves under static load to SLS loading, to ULS loading and to the onset of damage/failure have been obtained. Measured ultimate moments and rotational stiffnesses will be evaluated and modes of failure discussed. To execute the demonstrator house at Bourne, England, the frame joints had the detailing for SPJ-1.

Materials and Specimens

All components in the SLBS are pultruded shapes and are processed by EXEL Composites UK. Shown in Figures 3(a) and 3(b) are, with nominal dimensions (in mm), the closed cross-sections for the floor beam and the stud column members that were created within the design process. Both sections have conventional E-glass unidirectional and continuous filament mat reinforcements with a polyester based matrix (http://www.exelcomposites.com/).

Figure 4 shows details of a SPJ specimen, which is formed from a continuous stud column and a 'cantilever' floor beam. To make connections between the two members, four FRP dowels are to be inserted into 'tight-fitting' holes. A close-up in the joint region is given in Figure 5 for details and nominal dimensions.

For a moment lever arm of 1318 mm, Figures 1 and 4 show that a SPJ specimen has a beam of length 1600 mm. The horizontal distance from joint centre to where the vertical downward load is applied should be to where the point of contraflexure is; this point having been determined by a rigid joint frame analysis with the most severe SLS load case. It is noteworthy that to finalize the lever arm the distance was adjusted to ensure the SLS shear force and SLS joint moment co-existed together. This required a change from 1627 mm to 1318 mm. A beam length > 1320 mm was necessary to locate a steel loading plate on the top flange; this fixture was required to distribute, into the FRP thin-walled section, the vertical point load.

As seen in Figure 4 the height of the stud column is set at 2850 mm. The centre of the joint divides the column into two equal lengths of 1425 mm. Each length represents the distance from the joint centre to the point to contraflexure. There had to be a small difference because the location of the pin holes were dictated by the 101.6 mm (4 in.) centre-to-centre holes in the meccano steel sections used to construct the loading frame. As a result of this practical detailing a pin centre is 1368 mm from the joint's centre.

Because the structural engineering intention was to create joint stiffness by way of 'tight-fitting' FRP dowels it was necessary to measure connection geometry. The two sections for each SPJ specimen were labelled for hole dimension measurements, and the scheme is shown in Figures 6(a) and 6(b). Members numbered '1' are for specimen SPJ-1. Figure 6(a) has three parts for the South side, North side and a view for the top of the beam member. Figure 6(b), similarly, shows the scheme used with a stud column member. For example, label **B1-TLS** is for the **B**eam member in specimen SPJ-**1** and the hole at the **T**op **L**eft position in **S**outh wall. **SC2-BRN** is for the **S**tud **C**olumn member in SPJ-**2** and the hole at the **B**ottom **R**ight in **N**orth wall. A joint specimen has been assembled using a beam and a column member with the same number, for example, B2 and SC2 are for SPJ-2.

Members for SJP-1 were delivered, with pre-drilled holes by an external fabricator, to the structures laboratory at The University of Warwick. Members for the SPJ-2 were delivered without holes drilled and the connection holes were drilled and reamed using a Butler Hydrabore Horizontal Borer CNC machine in the School of Engineering workshop. The hole diameters were measured with a three point internal micrometer to the nearest ±0.01 mm. Diameters presented in Table 1 are for beams B1 and B2, and columns SC1 and SC2. In column (1) the hole positions on the South side are given on the left side (of each row), and those, followed by a comma, are for the associated hole positions on the North side. Beam and column member labels are given in columns (2) and (4). Presented in columns (3) and (5) are the measured diameters.

Minimum and maximum diameters of 31.07 mm and 31.30 mm for B1 are highlighted in bold in column (3). In column (5), the minimum and maximum diameters for holes in SC1 are 31.09 mm and 32.02 mm, respectively. For members B2 (column 3) and SC2 (column 5) it can be seen that their four holes per side have the smallest variation of < 0.1 mm, with the diameters in the narrow range of 29.98 mm to 30.07 mm.

Presented in Tables 2 and 3 are the distances between centres to pairs of holes. At the base of the tables are the means from four measurements. Column (1) defines the beam or stud member. Columns (2) and (3) report the horizontal centre-to-centre hole distances. The equivalent measurements for vertical and diagonal distances are given in columns (4) to (7). In all columns (2) to (7) the holes distance on the South side is given as the upper entry, followed below by the same distance measured on the North side. Centre-to-centre distances were established by adding to the distance between perimeters the two radii, which were obtained from the hole diameters reported in Table 1. Measurements in Tables 2 and 3 for members B1 and SC1 show that hole positioning varied; its is found to be constant in both members B2 and SC2.

Using a ±0.01 mm resolution micrometre the measured wall thicknesses for the members are reported in Tables 4 and 5. Column (1) is as per Tables 2 and 3, and column (2) gives the labels for the four dowel connections per joint. The three thicknesses, in column (3), are for measurements at 60º spacing around a hole's perimeter. Mean wall thicknesses are given in column (4). The overall mean wall thicknesses are highlighted using bold font text. It is seen from the data in Tables 4 and 5 that the shapes have a different web thickness on the South and North sides. For the beam the mean wall thicknesses from Table 4 are 4.66 mm (S) and 5.33 mm (N). From Table 5 the stud column gives 4.11 mm (S) and 5.07 mm (N). Results indicate that the beam has overall mean of 5.0 mm, whereas the stud column is lower at about 4.6 mm. These values show that the total wall thicknesses are a good match to the nominal design dimensions given in Figures 3(a) and 3(b).

To assemble a SPJ specimen a length of top and bottom flange from the beam is cut off (see Figure 6(a)) so that the two webs can go either side of the stud column's webs.

Figures 7(a) and 7(b) show two sets of FRP dowels with nominal diameters of 28.9 mm and 30.0 mm and a constant length of 100 mm. This length had been specified by the 74 mm width of the beam section (Figure 3(a)), with an addition of 13 mm on both sides. The dowels had been machined from a pultruded fibre E-glass solid rod of unidirectional roving reinforcement before being delivered to The University of Warwick. It can be seen in the photographs (in Figures 7(b)) that the 30 mm dowels have a head cap at one end. SPJ-1 was assembled using a set of 28.9 mm dowels and SPJ-2 with a set at 30.0 mm diameter.

With the design shear strength for the rod material equal to 60 N/mm^2 the minimum single plane shear resistance is 39 kN. A group of four dowels of 28.9 mm diameter, for the joint shown in Figure 5, will possess a moment resistance of 48 kNm due to material shear failure.

Details of Joints

Details for SPJ-1 and SPJ-2, with test instrumentation, are presented in Figures 1 and 5 and in the photographs in Figures 8 and 9.

Subtracting the 28.9 mm dowel diameter from the minimum and the maximum hole diameters in beam B1 (see Table 1) it is found that the clearance hole is in the range of 2.2 to 2.4 mm. This range is higher still, at 2.2 to 3.1 mm, for stud column SC1. It is found that the total relative clearance when joining members B1 and SC1 can be 4.4 to 5.5 mm. For a SLS vertical deflection limit of *L*/480 the required end rotation is 4.2 mrad (from 5346/480 = 11.1 and $11.1/2.673\times10^6$ = 4.2 mrad) for a simply supported beam under uniformly distributed load. If the dowels can freely move within these oversized holes the joint can rotate (ϕ) by 29 mrad (from $(4.4/153.7)\times10^3$ = 28.6 mrad), which clearly classifies it as pinned. Such inappropriate hole diameters deliver a simple joint, the exact opposite of what is required in the design process for the Startlink house frame in Figures 1 and 2. There were two reasons for the oversized holes and they are: poor communication meant the fabricator did not know what a 'tight fitting' hole diameter should be; the fabricator used hand held tools to drill poorly positioned and variable diameter holes.

The justification for the series of physical tests (Zafari 2013) was to assess different approaches that, at the same time of providing joint the highest stiffness would enable rapid erection of the superstructure from the 2.4 m wide floor and wall panels seen in Figure 2. Panel construction requires the insertion of 20 dowel connections per wall side or beam end. Each of the five frame joints with four dowels requires alignment of eight holes (they are labelled TLS, TRS, BLS, BRS, TLN, TRN, BLN and NRS) in both stud column and beam member. Given the alignment challenge faced for unrestrained dowel insertion an appropriate clearance hole size, say 0.3 mm, is essential if on-site assembly is to be practicable and the jointing is to have the highest rotational stiffness possible.

In an attempt to overcome the presence of the oversized hole clearance, another of the four SAJ specimens (Zafari 2013) was fabricated with a structural adhesive to fill-out the voiding between dowels and members. A liberal amount of Crestabond® M1-30, a methacrylate structural adhesive, was applied before inserting an adhesively coated dowel. This product (Scott Bader Adhesives 2013) is a toughened, two component acrylic adhesive, with gap filling capability up to 50 mm, designed for bonding (FRP) composites. It has tensile strength of 17 to 20 N/mm^2 (MPa), tensile modulus of elasticity of 0.75 to 1.0 kN/mm^2 and elongation > 100%. Prior to testing this SAJ specimen had been kept at about 20^{o}C for, at least, 48 hours to ensure full cure; Scott Bader recommends 24 hours at room temperature.

Zafari (2013) showed that the sole application of structural adhesive to pack-out clearance hole voiding did not provide adequate stiffness against the M-ϕ response being classified as a pinned joint. In other words, should oversized clearance holes be present, the joint's rotational stiffness is going to be far too low for a portal frame, and this structural limitation cannot be overcome simply by the liberal use of a structural adhesive to pack out the clearance voiding.

To fallow the joint detailing to possess a relatively 'high' rotational stiffness the authors considered two options that minimise (or eliminate) the influence of having oversized holes. These detailing options for SPJ-1 (Figure 8) and SJP-2 (Figure 9) are:

1. Combined fully bonded FRP dowels with extra adhesive bonding over the mating surfaces common to the beam and column members.
2. Have precisely positions holes with a maximum hole clearance of no greater than 0.3 mm; with this clearance size the unrestrained free rotation for having tight-fitting dowels, with adhesive coating, is significantly reduced to under 3 mrad.

Specimen SPJ-1 is for option 1 and was assembled with a set of 28.9 mm diameter dowels and members B1 and SC1. The two component epoxy paste adhesive Araldite® 2015 (Huntsman Advanced Materials 2013) was liberally applied over the North and South side surfaces between overlapping member surfaces that are 2 mm apart (over an area of 78000 mm^2 on the two side). This created a hybrid joint combining doweling and bonded connections. Araldite® 2015 has a tensile strength at 23^{o}C of 30 N/mm^2, a tensile modulus of 2.0 kN/mm^2 and elongation at break of 4.4%.

There were two reasons for not using the Crestabond® M1-30 adhesive for the extra bonding. The first was that this acrylic adhesive has half the tensile modulus of elasticity (Scott Bader Adhesives 2013). The second was the confidence gained from the application of Araldite® 2015 by Mottram and Zheng (1999) in increasing rotational stiffness in pultruded FRP beam-to-column joints. Prior to testing SJP-1 the specimen had been kept at 20^{o}C for, at least, 48 hours to make sure that the Araldite had achieved full cure; according to supplier Huntsman Advanced Materials (2013) it requires only 4 hours at room temperature.

To satisfy option 2, assembly of specimen SPJ-2 used a set of FRP dowels having nominal diameter of 30 mm. This joint is shown in Figure 9. From the hole diameters reported in Table 1 and hole centres in Tables 2 and 3 it is seen that there is an exact match between members B2 and SC2. Because diameters only deviated by 0.1 mm in 30.0 mm, this joint could be assembled using ‘tight-fitting’ dowels. To complete the fabrication the Crestabond® M1-30 adhesive is liberally placed around a hole circumference before an adhesively coated dowel is forced through the four holes to form the mechanical connection. Because of the tight tolerance on geometry it was necessary to use a light mallet to apply an impact force to overcome inherent (frictional) resistance to insertion.

To summarize the differences between SPJ-1 and SJP-2 their dowel connection configurations are listed in Table 6. The first column is for specimen labels. Entries in the second column are for the diameters of the FRP dowels and in the third column for the sizes of clearance hole. The last column in Table 6 emphasizes that SPJ-1 had extra structural adhesive connections over the mating surfaces between the webs of the floor beam and stud column.

Test Configuration and Test Procedure

The portal frame in Figure 1 was analyzed by D. Kendall (Optima Projects Ltd.) using the Engissol software (two-dimensional), with frame elements modelled along the members’ neutral axes for a single portal frame under SLS loading. The neutral axes for the shear-rigid elements are shown in Figures 1 and 3. Presented in Figure 5 are the maximum SLS actions at the centre of the joint. The design bending moment is 6.8 kNm and the vertical shear force is 5.1 kN. A load factor of 1.5 is applied to obtain the ULS design moment of 10.1 kNm. For any joint detailing to be acceptable there must be no irreversible damage when the ULS action is repeatedly applied.

Figure 4 illustrates the loading configuration used. The bending moment and vertical shear force due to a UDL beam loading is converted into a vertical point force applied at a horizontal distance of 1318 mm from the centre of joint. The reason for this lever arm length is explained in the section on Materials and Specimens. The top and bottom ends of the column in Figure 1 have pin connections that allow 'free' in-plane rotation. The reason for having pinned supports is to satisfy the physics that the only forces transferred at the points of contraflexure are shear and axial.

Figure 4 is used to present the locations of the instrumentation, consisting of three Accustar® electronic inclinometers, two displacement transducers (labelled DTB and DBB), twelve strain gages and load cell. Components of rotation (θ_1, θ_2 and θ_3) and axial displacement (DTB and DBB) are labelled in Figure 10. Measured by inclinometers C1, C2 and C3 are, respectively, the rotations (amplified for visualisation) of the stud column just above the top flange of the beam (θ_1), the joint (θ_2) and the beam (θ_3). C1 is placed on the actual centre line of the stud column that passes through the joint centre (see Figure 4). It is located just above the top flange of the beam for no interaction when there is flexural deformation. Inclinometer C2 is positioned at the centre of the dowel connection group, and this coincides with the intersection of the centre lines of the column and the beam member. The difference between the joint and the column rotations (i.e., $\theta_2 - \theta_1$) gives a measure of joint rotation ϕ_j. It is assumed that θ_1 is the same column rotation existing at the centre of the joint; this 'hidden' rotation cannot be measured. Inclinometer C3 is sited on the longitudinal centre line of the beam. It is worth mentioning that at this section of the beam, where the flanges have been cut away, the major axis second moment of area is a minimum at 1.97×10^6 mm^4. Placement of C3 is as close as practical to the joint's end so that the difference between θ_3 and θ_1 gives a measure of the beam rotation ϕ_b.

Relative horizontal movement of the beam at the top and the bottom of its flanges were measured by a pair of displacement transducers, designated as DTB and DBB with the vertical separation of 315 mm shown in Figure 10. The first letter, D denotes Displacement, and second and third letters are for show Top of the Beam and Bottom of the Beam, respectively. These two transducer readings were used to determine the rotational response of the beam from:

$$\phi_{\mathrm{L\,T,B}} = \arctan\left(\frac{lt + lb}{l}\right) \times 1000 \qquad \text{mrad} \qquad (1)$$

where *lt* and *lb* are the horizontal displacements measured by transducers DTB and DBB and *l* is their vertical separation. Because there was no significant difference in the moment-rotation curves using Equ. (1) or rotation θ_3 from C3 no results for $\phi_{\mathrm{L\,T,B}}$ are presented in this paper.

Twelve conventional 3 mm (FLA-3-11) single strain gages were used to obtain representative measurements of either 'bearing' strain at the dowel holes, or tensile or compressive strains in the top and bottom beam flanges. Positions for 10 of the 12 gages are shown in Figure 6(a). Eight of the gages are placed around the four joint holes at 1 mm distance away from the perimeter. As seen in Figure 6(a) four are on the North side and four on the South side having an orientation of 26º to match the theoretical direction for the resultant bearing force. The gage orientation was obtained from the vector of forces using conventional engineering analysis (Owens and Cheal 1989), which combines the joint moment and shear force components at SLS loading. Bearing strain measurements enabled the authors to evaluate the force distribution per dowel connection. Recorded bearing, tensile and compressive strains also provided results to identify and check for local failure mechanisms.

In real time the transducer readings were stored to an ORION 3531D Schlumberger data logger, which automatically recorded the specified values at each load/rotation increment, and after 5 minutes from application of a load or rotation increment. Rotations were recorded to a resolution of 0.02 mrad (linear to ±1% over a 10^{o} range) and axial displacements to ±0.01 mm.

Load was applied by means of a hanger assembly and a ball bearing placed in a semicircular socket at the centre of a steel loading plate. The use of a 12.7 mm ball bearing ensured vertical alignment of the load during a moment or rotation increment with minimal axial and lateral force components. The applied force was measured through a tension load cell, having capacity of 9 tonnes (i.e. 90 kN), and it was connected in series with manually operated (independent) hydraulic tension jacks.

Each SPJ specimen was deformed, under static load control, in increments of 0.5 kN (0.66 kNm), until the joint experienced SLS loading of 5.1 kN (or 6.8 kNm). The joint was next unloaded. After three reloading-unloading cycles to 6.8 kNm the joint was left under constant deformation for a period of 24 hours to find out if there was a change in stiffness. The specimen was then loaded, in increments of 0.66 kNm to its design ULS moment of 10.1 kNm. Prior to continuing loading in the post-ULS region, a specimen was subjected to three unloading-reloading cycles up to 10.1 kNm. A test was terminated when either the joint could no longer take an increased moment or when the rotational deformation was considered to be excessive.

The rotation of the joint ($\phi_j = \theta_2 - \theta_1$) and of the beam ($\phi_b = \theta_3 - \theta_1$) were used at each moment/rotation increment to determine their rotational stiffness from $S = M / \phi$. By plotting a change to the next M or ϕ increment could be informed by the current and previous equilibrium states of the specimen.

Results and Discussion

Plotted in Figures 11 and 12 are the 'joint' and 'beam' M-ϕ curves for specimens SPJ-1 and SPJ-2. The ϕ_j generated curves are given by the solid curves with labels SPJ-1′ and SPJ-2′ and the ϕ_b curves have dashed curves and labels SPJ-1″ and SPJ-2″. They were constructed by joining, with straight lines, the data points recorded at each load increment during the entire test procedure. These M-ϕ curves are crossed by two horizontal lines for the SLS and ULS design moments of 6.8 kNm (M_s) and 10.1 kNm (M_U). At each increment there is a pair of M-ϕ points, one taken immediately, after applying 'load' increment and the second after another five minutes had elapsed. This explains why the curves can have a saw-tooth appearance.

From the beginning of the test the solid line curve gives a stiffer response than the dashed line curve. The lowering in M, with time, shows that the joint's response is experiencing FRP viscoelastic relaxation and/or damage growth. As would be expected, the time reduction in M becomes more prominent as ultimate failure, at M_{fail}, is approached.

Figure 11 presented the M-ϕ curves for SPJ-1, which has dowel connections with oversized clearance hole of 2-3 mm (in both members) and extra adhesive bonding over the beam and column mating surfaces. It can be seen that the SPJ-1' and SPJ-1" responses are linear up to 29.1 and 24.1 kNm, with the former moment about three times M_U. In Figure 12 the characteristics for SPJ-2 show approximately linear response up to twice M_U. This second joint has relatively lower stiffness than SPJ-1.

First audible acoustic emissions were heard from SPJ-1 when M was 16.5 kNm, but with no visible sign of material failure. Curve SPJ-1" starts to go non-linear for M > 24.1 kNm, and it was observed that failure, in the form of a local buckle, had initiated in the bottom flange of beam. This flange deformation can (just about) be seen in the photographs in Figures 13(a) and 13(b). By increasing M in the post-failure region to 29.1 kNm the response of SPJ-1' remained linear and this result provides no evidence for there being joint failure within the column member. No further joint deformation was applied to SPJ-1 because there was a danger of specimen instability. ϕ_j was measured to be 1.5 mrad at 29.1 kNm, and this joint rotation is about 1/15th of ϕ_b on the beam side.

Figure 14 shows the unloading-reloading curves for SPJ-1 up to M_s (i.e. 6.8 kNm) for $\phi_{j,s}$ and $\phi_{b,s}$. The extra subscript of 's' is for SLS loading. These linear curves have been extracted from the SPJ-1' and SPJ-1" curves in Figure 11. Cyclic loading was part of the test procedure, because the 'joint' and 'beam' stiffnesses on reloading might be more representative of what is to exist in a Startlink house. With both curves the linear trend line's equation, and R^2 (for linear regression fit), are reported in the figure. Values of R^2 > 0.91 show there to be an acceptable linear relationship. From the SLS curves in Figure 14 the rotational stiffnesses for the joint is 15700 kNm/rad ($S_{j,s}$) and for the beam it is 1590 kNm/rad ($S_{b,s}$). It is found that $S_{j,s}$ was about ten times higher than $S_{b,s}$. Figure 15, similarly, shows for zero moment to M_U the joint rotation ($\phi_{j,U}$) and beam rotation ($\phi_{b,U}$). New subscript 'U' is for ULS loading. At the design ULS moment $S_{j,U}$ and $S_{b,U}$ are calculated to be 18700 kNm/rad and 1560 kNm/rad, respectively. It was found that there is a negligible increase (change) in measured rotations when SPJ-1 was unloaded and reloaded and, therefore, the response can be assumed to remain linear and elastic and repeatable to M_U.

It is believed that moment was transferred from the beam into the stud column through the bonded connection. The four dowels can be assumed to remain relatively unloaded until the adhesive fails, which it did not. Let us now assume the Araldite 2015® bonded connection had completely failed at *M* equals 29.1 kNm and so the dowels were left to resist this 'failure' moment. The shear force taken by each dowel would be 47.3 kN (= 29100/(4×153.7)). The first number in brackets is $M_{j,fail}$ in kNmm, the second is the number of dowels and the third is the distance from joint centre to each dowel centre. As a result the average shear stress would be 36 N/mm^2 (= 47.3×1000/656×2). The denominator is cross-section area (in mm^2) for a 28.9 mm diameter dowel, times two for the two shear planes. This average shear stress is below the design material shear strength of 60 N/mm^2.

Figure 16 shows the moment-strain (M-ε) curves plotted from strains from the South-side gages of TLS (medium dashed line), TRS (long-dashed line), BLS (short dashed line) and BRS (dotted line). The positions of these gages around the four holes are seen in Figure 6(a). The axial strain was compression. It can be seen from the figure that the maximum bearing strain, when *M* is 29.1 kNm, is about 0.004 (or 4000 με), and that it occurs close to hole TRS. The relatively low bearing strains in SPJ-1 indicate that the joint moment had effectively been transferred through the bonded connection.

Because there is a complex stress field in the region where the connection (bearing) force is transferred between the FRP dowel and the wall of beam's web the compressive strain for bearing failure is an unknown mechanical property. It may be assumed that the compressive strain recorded by the strain gage would need to exceed 0.01 for there to be bearing failure. This assessment is valid only when the resultant connection force is aligned with the orientation of the strain gage.

It is acceptable to observe that failure of specimen SPJ-1 is related to geometry and methods of connection, and not because of a pultruded FRP material strength. Another piece of evidence to support this finding is that the joint's stiffness (M/ϕ_j) remained linear to 29.1 kNm.

Let's now assess the structural performance of specimen SPJ-2. Plotted in Figure 12 are the M-ϕ curves for a joint with a configuration having 'tight-fitting' dowel connections. This specimen had been fabricated by the authors to imitate the situation that the frame joint would experience with ideal FRP dowel connections for the stiffness joint. The detailing represents the stiffness and strongest that can be fabricated without the addition of the Araldite 2015® adhesive bonding, as per SPJ-1.

It is seen that the M-ϕ responses for both SPJ-2' and SPJ-2" remains, perfectly, linear until M was about 16.5 kNm. Audible acoustic emissions were then heard, without there being any visible sign of material failure. Behavior stayed, approximately, linear until M was 20.4 kNm, when there were bond fractures, local to the TRN and BRN dowel connections. It was observed that immediately after adhesive failure there was localized bearing failure too. As the joint lost its structural integrity and the moment continually reduced there was progressive material failure leading to excessive web deformation and outward curl of the beam's top flange. The shape of the M-ϕ curves after 20.4 kNm in Figure 12 corresponds to the observed failure process. Bearing failure at connection TRN and the excessive beam deformation on the North side of SPJ-2 are shown in Figures 17(a) and 17(b).

Figure 18 presents the unloading-reloading M-ϕ curves for SPJ-2 to M_s for $\phi_{j,s}$ and $\phi_{b,s}$ measurements. Figure 19 gives the same joint's M-ϕ results up to M_U. These curves, for three cyclic loadings, were extracted from the SPJ-2' and SPJ-2" curves in Figure 12. It is found that there was a negligible increase in ϕ_j and ϕ_b when SPJ-2 was unloaded and reloaded and, therefore, the response remained elastic and repeatable throughout. The R^2 values are 0.94 or higher for the linear trend lines. This shows that rotational stiffness is fairly constant to M_U. From the curve fits in Figure 18 the SLS rotational stiffness is 2650 kNm/rad ($S_{j,s}$) and for the beam it is 1300 kNm/rad ($S_{b,s}$). Using the test results in Figure 19, $S_{j,U}$ and $S_{b,U}$ are 2190 kNm/rad and 1150 kNm/rad, respectively. For SPJ-2 the difference between the joint and beam stiffnesses are no more than doubled, much less than found with SPJ-1.

Figure 20 presents the M-ε curves at the four connections of TLS (medium dashed line), TRS (long dashed line), BLS (short dashed line) and BRS (dotted line). It is noted that the two curves for BLS and BRS coincide. Although full bearing failure was observed at TRN and BRN the highest bearing strains were measured at TRS and BRS. It is observed that when M is 20.4 kNm the maximum bearing strain of 0.01 (or 10300 με) is at gage TRS. A plausible explanation is given below for why the bearing failure in the beam web may not be associated with the highest measured bearing strain.

Comparing the bearing strains at gages TLS, TRS, BLS and BRS for SPJ-2 (Figure 20) and SPJ-1 (Figure 16) it is found that, at the same *M*, the direct strains in SPJ-2 are about 3 to 6 times higher. This finding again indicates that the moment and shear force in joint SPJ-1 had effectively been transferred through the extra bonding between mating surfaces.

The authors believe that audible acoustic emissions (heard when *M* was about 16.5 kNm) might possibly be related to the initiation of bearing failure in the stud column walls. The reason for this observation is that this wall has a nominal thickness of 4.5 mm, which is 0.5 mm lower than for the beam's web. Because the same connection force is resisted by both wall thicknesses failure is most likely to happen in the stud's walls first.

Another finding from testing SPJ-2 is the influence of using Cestabond® M1-30 with the doweling. This adhesive was applied liberally on dowel insertion and so partially filled the voiding from having a 2 mm gap between the members B2 and SC2. Figure 21(a) and 21(b) show that there was a different plug area around each of the four dowels. The minimum area had a diameter of about 1.2 times the hole diameter (30 mm) and the maximum area had a diameter of at least 2 times. It was found that a dowel connection with the minimal bonding experienced bearing failure first on the stud column side. The authors believe that until the plug bond failed there was no FRP material deterioration.

It is obvious that once the 2 mm thick layer of Crestabond® M1-30 debonds from one of the members, it remained attached to the other member. As a result of this failure process one of the two walls experienced an effective increase in thickness, and thereby a reduced mean bearing stress. This can explain where bearing failure occurs. Figures 21(a) and 21(b) show the South and North sides of SPJ-2 after dismantling to inspect the failure zone. Figure 21(a) shows that the connections at TRS and BRS on the stud column side had failed in bearing. It can be seen that around these two holes less adhesive had been applied. Consequently, they had relatively a higher mean bearing stress than at dowel connections TLS and BLS. It is possible that these two connections experienced a bearing force that was 10% lower. No bearing failure was observed along the other six hole perimeters on the South side. On the

North side, as can be seen from Figure 21(b) the more severe bearing stress field belonged to TRN and BRN in the beam's web. Again, this finding is because plug failure changed the effective size of the bearing area within the dowel connections.

Joint Properties and Classification

Collated in Tables 7 and 8 are measured joint properties from SPJ-1 and SPJ-2 using, respectively, joint rotation ϕ_j and beam rotation ϕ_b. In these two tables column (1) gives the specimen label. Initial joint properties are given in columns (2) to (4), and are represented by initial moment ($M_{j,int}$), initial rotation ($\phi_{j,int}$) and initial stiffness ($S_{j,int} = M_{j,int} / \phi_{j,int}$). $M_{j,int}$ and $\phi_{j,int}$ are from measurements during the loading procedure over the M increments of 0.66 kNm to 1 kNm. The SLS moment properties of $\phi_{j,s}$ and $S_{j,s}$ with corresponding moment $M_{j,s}$ are reported in columns (6) and (7) respectively. Similarly, $\phi_{j,u}$ and $S_{j,u}$ for ULS moment ($M_{j,u}$) are reported in columns (9) to (10). $S_{j,s}$ and $S_{j,u}$ are the secant stiffnesses at SLS and ULS moments, taken from the curves plotted in Figures 14, 15, 18 and 19.

Columns (5), (8) and (11) in Table 7 report values for $k_{j,int}$, $k_{j,s}$ and $k_{j,u}$ using the joint rotation. These non-dimensional stiffnesses are obtained by dividing the rotational stiffness of $S_{j,int}$, $S_{j,s}$ and $S_{j,u}$ by the flexural stiffness of the beam member (i.e. $E_{beam}I_{beam}/L_{beam}$). The equivalent of $k_{b,int}$, $k_{b,s}$ and $k_{b,u}$ from the beam rotation are given in the same columns in Table 8. E_{beam} is the (longitudinal) flexural modulus of elasticity and I_{beam} is the major axis second moment of area of the beam member in Figure 3(a). L_{beam} is for the floor span, which from Figure 1 is 5350 mm (taken from centroid axis to centroid axis of the columns). I_{beam} for the floor beam member (with floor panel (Zafari 2013)) in Figure 3(a) is 58.3×10^6 mm^4 and E_{beam} is taken to be 24 kN/mm^2.

Reported in columns (12) and (13) are the maximum moment (M_{max}) and corresponding maximum rotation (ϕ_{max}). These joint properties were defined when the response of SPJ' and SPJ" curves started to go non-linear. The last column (14) is used to list the moment at ultimate failure (M_{fail}).

Comparing the rotational stiffnesses from the joint rotation and beam rotation given in columns (4), (7) and (10) of Tables 7 and 8, it is observed that the flexibility on the beam side was about 6 times to 12 times higher.

According to clause 5.2.2 in BS EN 1993-1-8:2005 (British Standards Institution 2005) an unbraced (steel) frame joint is classified as rigid, if $k_{beam} \geq 25$, when $S_{j,int} \geq k_{beam}E_{beam}I_{beam}/L_{beam}$, provided that in every storey $K_{beam}/K_{column} \geq 0.1$. K_{beam} is the mean value of I_{beam}/L_{beam} for all the beams at the top of that storey and K_{column} is the equivalent value for the columns in that storey. This condition is satisfied by the Startlink house frame and members shown in Figures 1 and 3.

Calculated $k_{j,int}$, $k_{j,s}$ and $k_{j,u}$ values in columns (5), (8) and (11) of Table 7 for SPJ-1 are 34, 60 and 71 respectively. The beam-side equivalents of $k_{b,int}$, $k_{b,s}$ and $k_{b,u}$ from Table 8 give a constant of 6. On the joint-side SPJ-1 classifies as a rigid joint because $k_{j,int}$ is greater than 25. It found to be semi-rigid on the beam-side.

For SPJ-2 the same three k_js in Table 7 for ϕ_j are in the range of 11 down to 8. The equivalent k_bs in Table 8 range from 6 down to 4. Applying the classification process the joint details in SPJ-2 are for a semi-rigid joint that cannot provide adequate rotational stiffness to satisfy the Startlink frame design assumption for having rigid joints.

Results for SPJ-2 confirm the finding that the presence of 'tight fitting' dowel connections, without extra adhesive bonding, cannot provide adequate joint stiffness. There are weaknesses with the engineering solution of introducing a structural adhesive for the extra bonding, as in specimen SJP-1, connecting the webs of the beam and stud column. One weakness is that on-site fabrication is a formidable task, especially with the need to deliver quality bonding in, for example, adverse weather conditions. Another weakness is that once bonded the joint cannot readily be disassembled for reuse. An option to overcome the challenges of finding practical details for a rigid joint in the Startlink portal frame (Figures 1 and 2) is to develop a vertical bracing system, such as commonly found in frame construction with structural steel.

Concluding Remarks

Two unique physical tests have been conducted under static load to provide indicative test results on the moment-rotation characteristics and to establish the mode(s) of failure for practical joints in the Startlink house portal frame. Using the results an evaluation is made on the performance of the joints with regards to design moments and the design requirement for a rigid rotational stiffness. Both joint specimens had FRP dowel connections with or without hole clearance and the joint with hole clearance had extra adhesive bonding on common surfaces between the members. Both dowels and the perimeter of the holes were coated with a structural adhesive before assembling the joint to provide a level of continuity in the presence of hole clearance.

The following are salient results from the static testing that can be used to develop an overall understanding of the unbraced Startlink house frame with regard to its overall stiffness and structural performance:

- Joint moment at failure is in excess of the ULS design moment given by multiplying the SLS design moment by the chosen partial load factor of 1.5. The most severe loading case generates a SLS joint moment of 6.8 kNm; the accompanying shear force is 5.1 kN.
- According to the classification process in BS EN 1993-1-8:2005 (British Standards Institution 2005), the joint with the extra bonded connection between overlapping surfaces of the members is rigid. The second joint, having tight fitting dowel connections and no extra bonding between the overlapping surfaces, is found to be semi-rigid, and there is every likelihood this joint is too flexible for the Startlink house.
- The moment-rotation curve for the stiffer (rigid) joint detailing was found to be linear to a moment of 29.1 kNm, which is about three times higher than the ULS moment. It was observed that joint failure was related to geometry and methods of connection, and not because of composite material strength. Measurements of bearing strain at the dowel connections indicated that the joint moment and shear force were effectively transferred through the extra bonded connection and not by way of the FRP dowels.
- The moment-rotation curves for the more flexible joint showed it remained linear to a moment of 20.4 kNm; which is twice the ULS moment. There might have been material damage when the moment was 1.5 times the ULS moment. In order of visual observation the failure modes were plug bond fracturing around the dowel connections, connection bearing failure and, finally, top flange curl and excessive web flexural deformation.

- Rotational stiffnesses for the joint having tight fitting dowels indicates that without extra adhesive bonding a rigid rotational stiffness is not achievable. Given that there are practical weaknesses with having to reply on a structural adhesive to develop the necessary rotational stiffness the authors recommend that the Startlink house frame be further developed to have an integrated vertical bracing system.

Acknowledgements

The authors thank EXEL Composites UK for supplying the components for the portal frame joint sub-assemblies. The partners who worked on *Startlink Lightweight Building System* project (2009-2012) are grateful to the Technology Strategy Board (TSB) for UK Government's support via the Low Impact Buildings' Innovation Platform. Appreciation is given to Mr D. Kendall of Optima Projects Ltd., UK, for carrying out the design calculations that informed the creation of the structural form and bespoke pultruded shapes. The authors thank Mr C. Bank, Mr R. Bromely and Mr G. Canham in the School of Engineering for providing essential technical support.

References

Anonymous. (2007). *Homes for future: more affordable, more sustainable - Housing Green Paper.* Communities and local Government publications, Wetherby, England. http://webarchive.nationalarchives.gov.uk/+/http:/www.communities.gov.uk/publications/housing/homesforfuture (31 August 2013)

Bank, L. C. (2006). *Composites for construction - Structural design with FRP materials*, John Wiley & Sons, New Jersey.

British Standards Institution (1997). *Loading for buildings - Part 2: Code of practice for wind loads*, *BS 6399-2:1997,* London.

British Standards Institution (2005). *Eurocode 3: Design of steel structures - Part 1-8: Design of joint, BS EN 1993-1-8:2005,* London.

Clarke, J. L. Ed. (1996). *Structural design of polymer composites: EUROCOMP design code and background document,* E. & F.N. Spon, London.

Huntsman Advanced Materials. (2013). *Araldite® 2015 Structural adhesive*, Technical data sheet. http://www.intertronics.co.uk/data/ara2015.pdf (31 August 2013)

Hutchinson, J. and Hartley, J. (2011). "STARTLINK lightweight building system – Wholly polymeric structures." *Proc. 5th Inter. Conf. on Advanced Composites in Construction (ACIC 2011)*, Net Composites, Chesterfield, 355-363.

Mottram, J. T. and Zheng, Y. (1999). "Further tests of beam-to-column connections for pultruded frames: flange-cleated." *J. Compos. Const.*, **3** (3), 108-116.

Owens, G. W. and Cheal, B. D. (1989). *Structural steelwork conne*ctions, Butterworth-Heinemann, London.

Scott Bader Adhesives. (2013). *Crestabond® M1-30 - Methacrylate structural adhesive*. http://www.scottbader.com/uploads/files/885_crestabond-m1-30-crestabond-en-feb13.pdf (31 August 2013)

Singleton, M. (2004). *Startlink system of pultruded GRP profiles for structural systems*. International Patent Application No. PCT/GB2004/003832.

Singleton, M. and Hutchinson, J. (2007). "*STARTLINK composite housing*." www2.warwick.ac.uk/fac/sci/eng/staff/jtm/paper_startlink.pdf (31 August 2013)

Zafari, B. (2013). *Startlink building system and connections for fibre reinforced polymer structures*, PhD thesis, The University of Warwick, UK.

Table captions

Table 1. Diameters of holes in Startlink floor beams and stud columns.

Table 2. Horizontal, vertical and diagonal hole distances in beam members B1 and B2.

Table 3. Horizontal, vertical and diagonal hole distances in stud column members SC1 and SC2.

Table 4. Mean thicknesses of walls in Startlink floor beam shape.

Table 5. Mean thicknesses of walls in Startlink stud column shape.

Table 6. Dowel connection configurations in specimens SPJ-1 and SPJ-2.

Table 7. SPJ′s properties from joint rotation ϕ_J.

Table 8. SPJ″s properties from beam rotation ϕ_b.

Figure captions

Figure 1. Startlink portal frame with specimen SPJ for external frame joint at first floor level.

Figure 2. Startlink superstructure showing panels, members and frame joints.

Figure 3. Startlink shapes: a) floor beam; b) stud-column.

Figure 4. SPJ specimen with dimensions and test instrumentation.

Figure 5. SPJ connections and joint actions from the most severe SLS load case.

Figure 6. Engineering drawings: (a) beam with holes positions and the nominal distances between pairs of holes; (b) stud column with holes positions and the nominal distances between pairs of holes.

Figures 7. Two sets of dowels: (a) for SPJ-1; (b) for SPJ-2.

Figures 8. SPJ-1 viewed from the South side.

Figures 9. SPJ-2 viewed from the South side.

Figure 10. SPJ with the position of displacement transducers, inclinometers and defining the rotations.

Figure 11. M-ϕ curves for SPJ-1.

Figure 12. M-ϕ curves for SPJ-2.

Figures 13. SPJ-1 failure mode; (a) whole specimen, (b) local to compression flange adjacent to the dowelling and adhesive bonding.

Figure 14. Cyclic M-ϕ curves up to the design SLS moment for SPJ-1.

Figure 15. Cyclic M-ϕ curves up to the design ULS moment for SPJ-1.

Figure 16. M-ε curves for SPJ-1.

Figure 17. SPJ-2 failure mode: (a) bearing failure; (b) beam web local buckling.

Figure 18. Cyclic M-ϕ curves up to the design SLS moment for SPJ-2.

Figure 19. Cyclic M-ϕ curves up to the design ULS moment for SPJ-2.

Figure 20. M-ε curves for SPJ-2.

Figure 21. SPJ-2 debonding and bearing failures: (a) South view; (b) North view.

Table 1. Diameters of holes in Startlink floor beams and stud columns.

Position	Member	Measured diameter (mm)	Member	Measured diameter (mm)
(1)	(2)	(3)	(4)	(5)
TLS, TLN	**B1**	31.17 , 31.22	**SC1**	**32.02** , 31.13
TRS, TRN		31.21 , 31.27		31.57 , **31.09**
BLS, BLN		**31.07** , 31.18		31.67 , 31.77
BRS, BRN		31.17 , **31.30**		31.12 , 31.18
TLS, TLN	**B2**	29.99 , 30.04	**SC2**	29.99 , 30.03
TRS, TRN		29.99 , 30.05		29.98 , 30.04
BLS, BLN		**29.98** , 30.06		30.03 , **30.07**
BRS, BRN		29.99 , 30.04		29.99 , 30.03

Table 2. Horizontal, vertical and diagonal hole distances in beam members B1 and B2.

Member		Horizontal distance		Vertical distance		Diagonal distance	
(1)		(2)	(3)	(4)	(5)	(6)	(7)
		TL-TR	BL-BR	TL-BL	TR-BR	TL-BR	TR-BL
B1	S	266.1	265.2	153.2	153.3	307.2	307.1
	N	266.2	265.3	154.1	154.2	306.3	307.2
B2	S	266.0	266.0	154.0	154.0	307.4	307.4
	N	266.0	266.0	154.0	154.0	307.4	307.4
Mean		261.1	265.6	153.8	153.9	307.1	307.3

Table 3. Horizontal, vertical and diagonal hole distances in stud column members SC1 and SC2.

Member		Horizontal distance		Vertical distance		Diagonal distance	
(1)		(2)	(3)	(4)	(5)	(6)	(7)
		TL-TR	BL-BR	TL-BL	TR-BR	TL-BR	TR-BL
SC1	S	264.8	266.3	153.8	152.9	307.1	306.6
	N	266.5	265.1	153.1	154.5	306.6	308.4
SC2	S	266.0	266.0	154.0	154.0	307.4	307.4
	N	266.0	266.0	154.0	154.0	307.4	307.4
Mean		265.8	265.9	153.7	153.9	307.1	307.5

Table 4. Mean thicknesses of walls in Startlink floor beam shape.

Specimen	Hole	Measured thickness (mm)			Mean (mm)
(1)	(2)	(3)			(4)
B1	TLS	4.90	4.67	4.84	4.80
	TLN	5.21	5.08	5.72	5.34
	TRS	4.27	4.68	4.52	4.49
	TRN	5.44	5.67	5.55	5.55
	BLS	4.64	4.41	4.77	4.61
	BLN	5.27	5.05	5.16	5.16
	BRS	4.27	4.67	4.46	4.47
	BRN	5.44	5.39	5.66	5.50
				Mean for B1	**4.99**
B2	TLS	4.67	4.87	4.88	4.81
	TLN	5.16	5.28	5.31	5.25
	TRS	4.69	4.88	4.92	4.83
	TRN	5.23	5.23	5.11	5.19
	BLS	4.75	4.70	4.42	4.62
	BLN	5.31	5.22	5.05	5.19
	BRS	4.49	4.61	4.75	4.62
	BRN	5.56	5.31	5.52	5.46
				Mean for B2	**5.00**

Table 5. Mean thicknesses of walls in Startlink stud column shape.

	Specimen	Measured thickness (mm)			Mean (mm)
(1)	(2)	(3)			(4)
SC1	TLS	4.16	4.23	4.21	4.20
	TLN	4.97	4.88	4.90	4.92
	TRS	4.10	4.16	4.20	4.15
	TRN	5.04	4.88	4.96	4.96
	BLS	3.95	4.07	3.94	3.99
	BLN	5.12	5.24	5.17	5.18
	BRS	3.92	4.06	3.85	3.94
	BRN	5.16	5.21	5.24	5.20
				Mean for SC1	**4.56**
SC2	TLS	4.12	4.23	4.31	4.22
	TLN	5.29	5.03	4.99	5.10
	TRS	3.98	3.94	4.09	3.97
	TRN	5.17	5.28	5.18	5.21
	BLS	4.28	4.40	4.36	4.35
	BLN	4.89	4.96	4.68	4.84
	BRS	3.92	4.07	4.16	4.05
	BRN	5.14	5.22	5.03	5.13
				Mean for SC2	**4.61**

Table 6. Dowel connection configurations in specimens SPJ-1 and SPJ-2.

Specimens	Dowel diameter (mm)	Hole clearance (mm)	Bonded connection
(1)	(2)	(3)	(4)
SPJ-1	28.9	2-3	Between overlapping surfaces of the members
SPJ-2	30.0	‘tight fit’	N/A

Table 7. SPJ′s properties from joint rotation ϕ_j .

Specimen	$M_{j,int}$ (kN m)	$\phi_{j,int}$ (mrad)	$S_{j,int} = M_{j,int} / \phi_{j,int}$ kN m/rad	$k_{j,int}$	$\phi_{j,s}$ (mrad)	$S_{j,s} = M_s / \phi_{j,s}$ kN m/rad	$k_{j,s}$	$\phi_{j,U}$ (mrad)	$S_{j,U} = M_U / \phi_{j,U}$ kN m/rad	$k_{j,U}$	$M_{j,max}$ (kN m)	$\phi_{j,max}$ (mrad)	$M_{j,fail}$ (kN m)
(1)	(2)	(3)	(4)	(5)	(6)	(7)	(8)	(9)	(10)	(11)	(12)	(13)	(14)
SPJ-1′	1.34	0.2	9000	34	0.4	15700	60	0.5	18700	71	29.1	1.5	29.1
SPJ-2′	1.33	0.5	2950	11	2.6	2650	10	4.7	2190	8	20.4	11.2	20.4

Table 8. SPJ″s properties from beam rotation ϕ_b.

Specimen	$M_{j,int}$ (kN m)	$\phi_{b,int}$ (mrad)	$S_{b,int} = M_{j,int} / \phi_{b,int}$ kN m/rad	$k_{b,int}$	$\phi_{b,s}$ (mrad)	$S_{b,s} = M_s / \phi_{b,s}$ kN m/rad	$k_{b,s}$	$\phi_{b,U}$ (mrad)	$S_{b,U} = M_U / \phi_{b,U}$ kN m/rad	$k_{b,U}$	$M_{b,max}$ (kN m)	$\phi_{b,max}$ (mrad)	$M_{b,fail}$ (kN m)
(1)	(2)	(3)	(4)	(5)	(6)	(7)	(8)	(9)	(10)	(11)	(12)	(13)	(14)
SPJ-1″	1.34	0.9	1490	6	4.4	1590	6	6.8	1560	6	24.1	17.0	29.1
SPJ-2″	1.33	0.9	1550	6	5.4	1300	5	9.1	1150	4	20.4	19.2	20.4

Notes: M_S is 6.8 kN m and M_U is 10.1 kN m

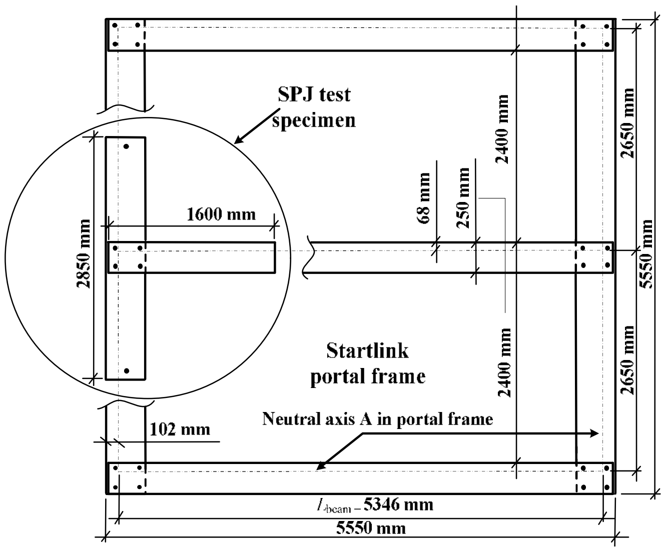

Figure 1. Startlink portal frame with specimen SPJ for external frame joint at first floor level.

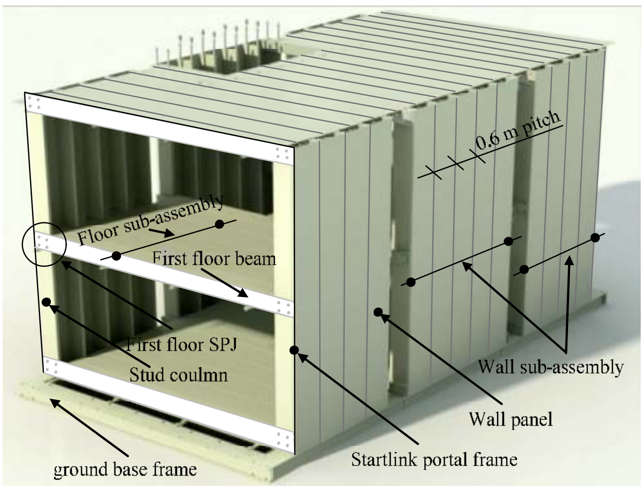

Figure 2. Startlink superstructure showing panels, members and frame joints.

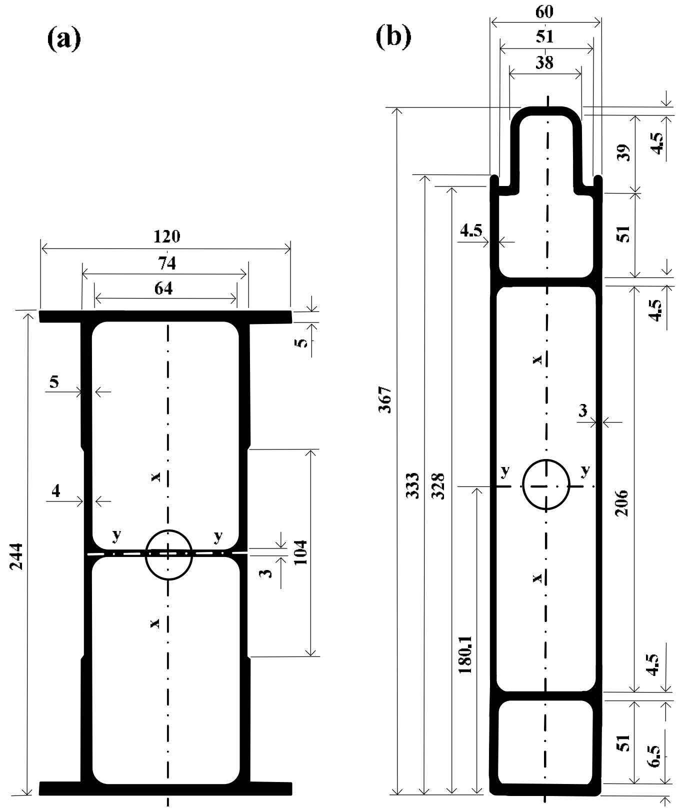

Figure 3. Startlink shapes: a) floor beam; b) stud-column .

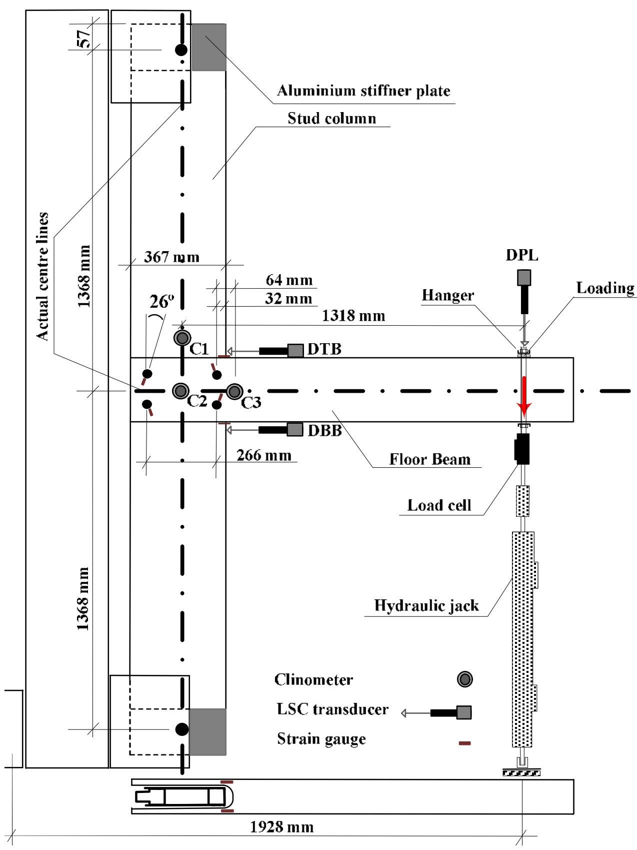

Figure 4. SPJ specimen with dimensions and test instrumentation.

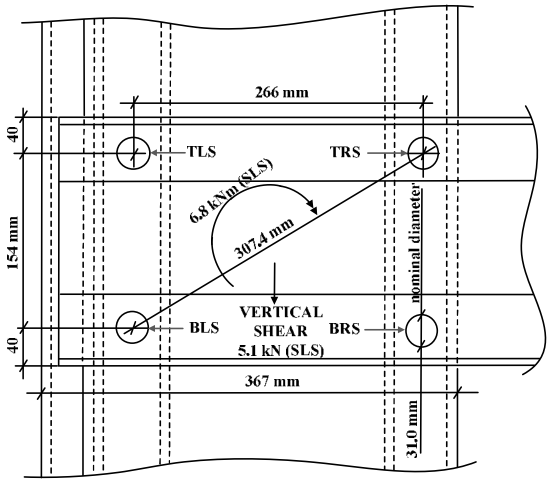

Figure 5. SPJ connections and joint actions from the most severe SLS load case.

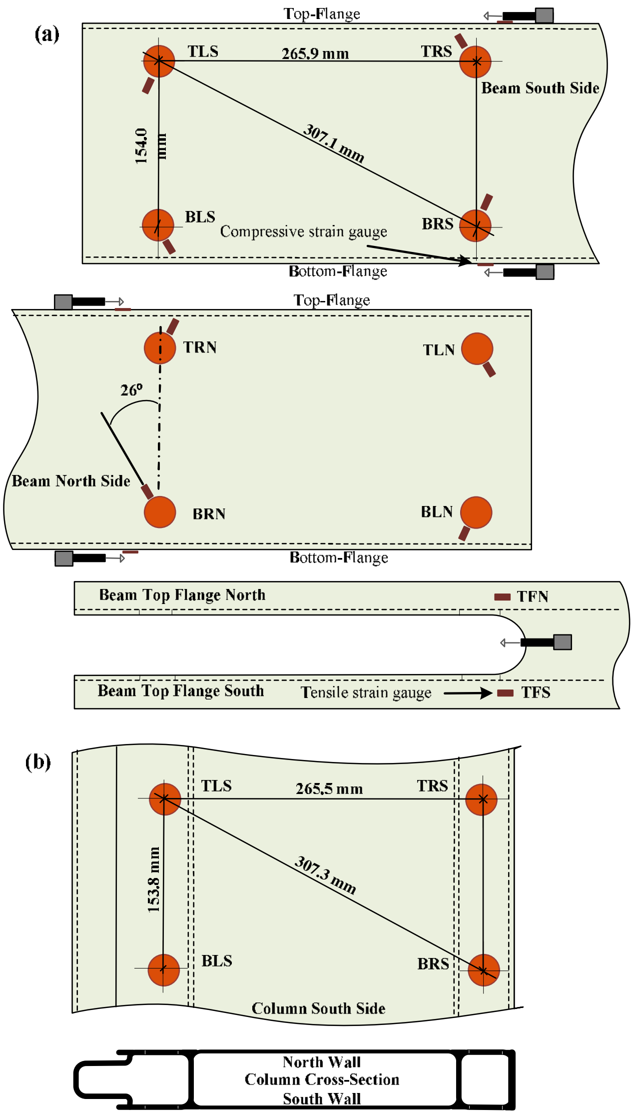

Figure 6. Engineering drawings: (a) beam with holes positions and the nominal distances between pairs of holes; (b) stud column with holes positions and the nominal distances between pairs of holes.

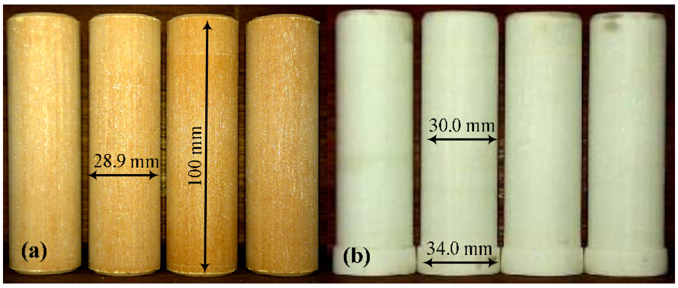

Figures 7. Two sets of dowels: (a) for SPJ-1; (b) for SPJ-2.

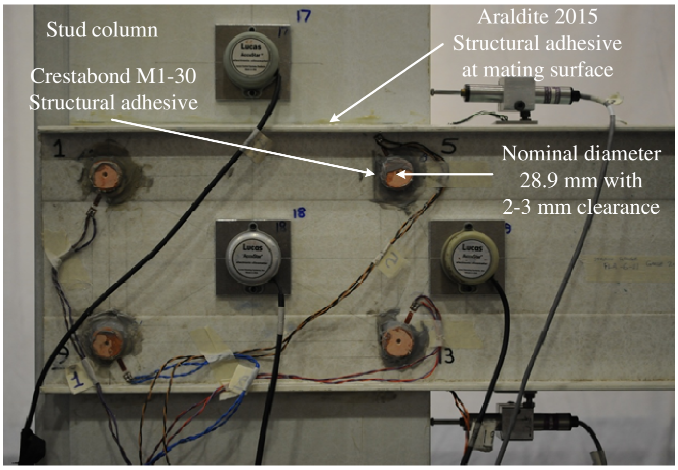

Figures 8. SPJ-1 viewed from the South side.

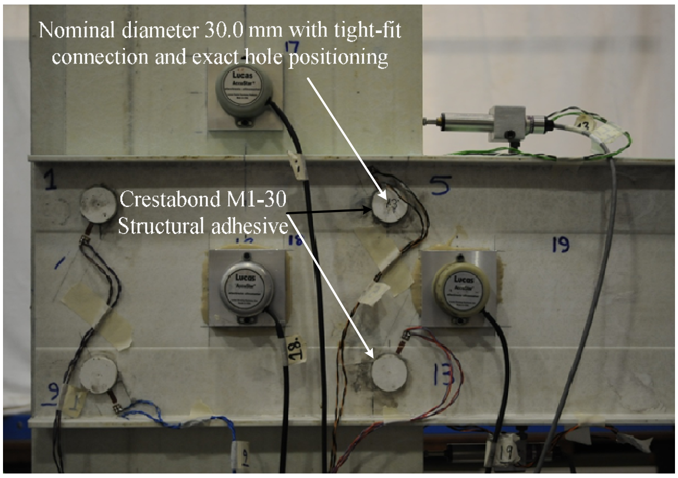

Figures 9. SPJ-2 viewed from the South side.

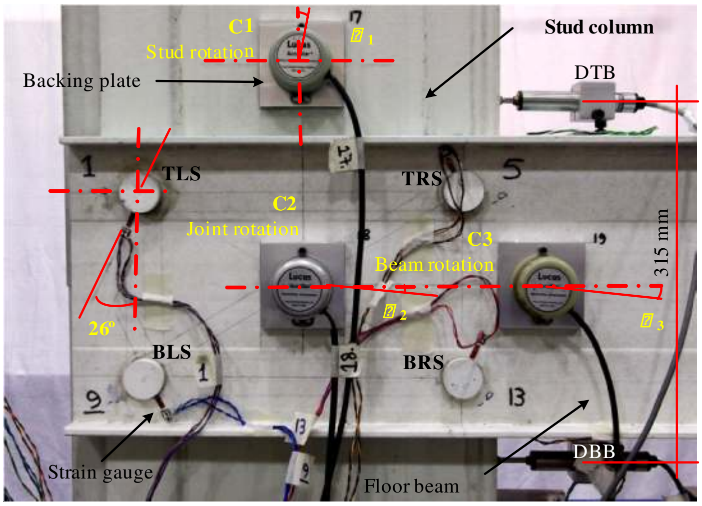

Figure 10. SPJ with the position of displacement transducers, inclinometers and defining the rotations.

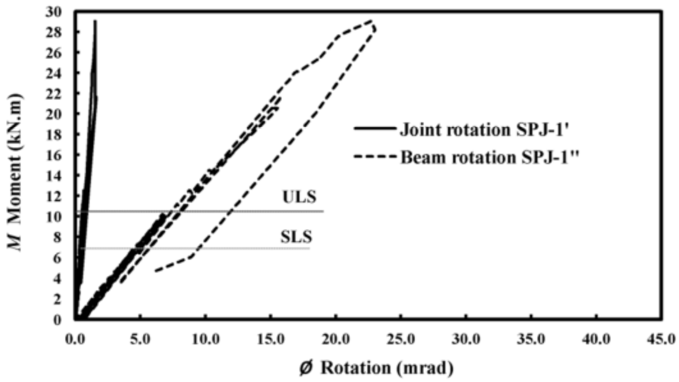

Figure 11. M-ϕ curves for SPJ-1.

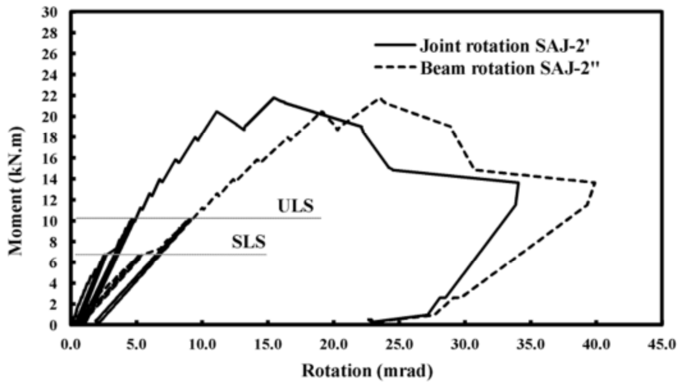

Figure 12. M-ϕcurves for SPJ-2.

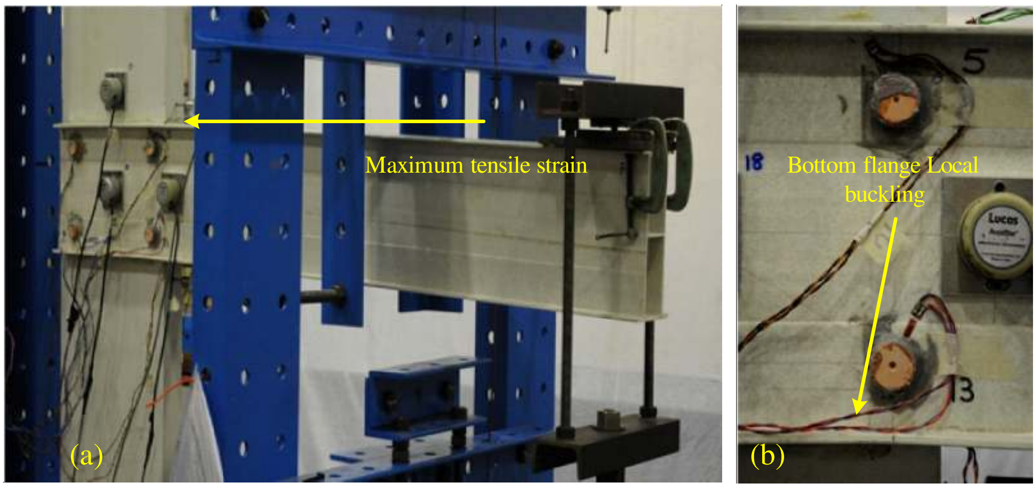

Figures 13. SPJ-1 failure mode; (a) whole specimen, (b) local to compression flange adjacent to the dowelling and adhesive bonding.

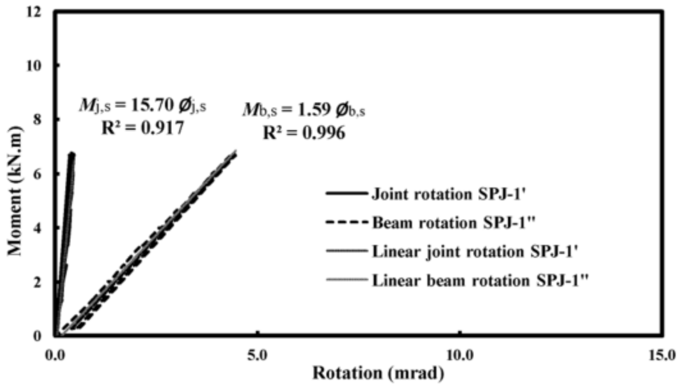

Figure 14. Cyclic M-ϕ curves up to the design SLS moment for SPJ-1.

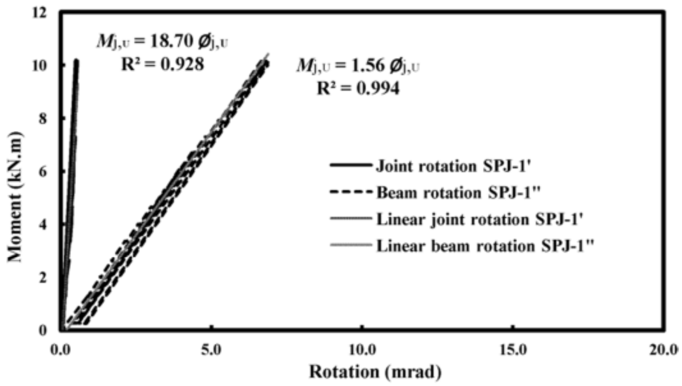

Figure 15. Cyclic M-ϕ curves up to the design ULS moment for SPJ-1.

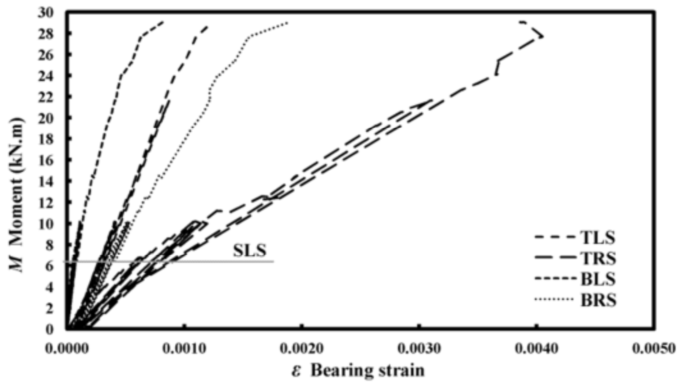

Figure 16. M-ε curves for SPJ-1.

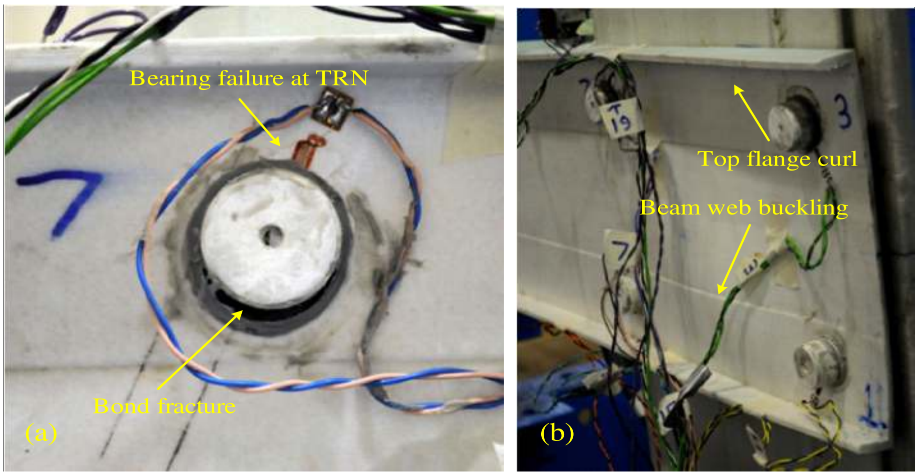

Figure 17. SPJ-2 failure mode: (a) bearing failure; (b) beam web local buckling.

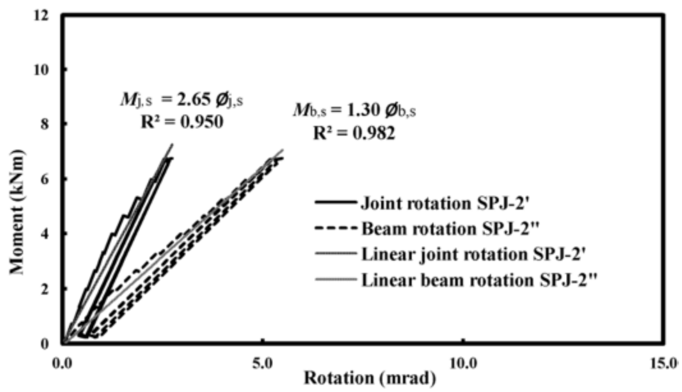

Figure 18. Cyclic M-ϕ curves up to the design SLS moment for SPJ-2.

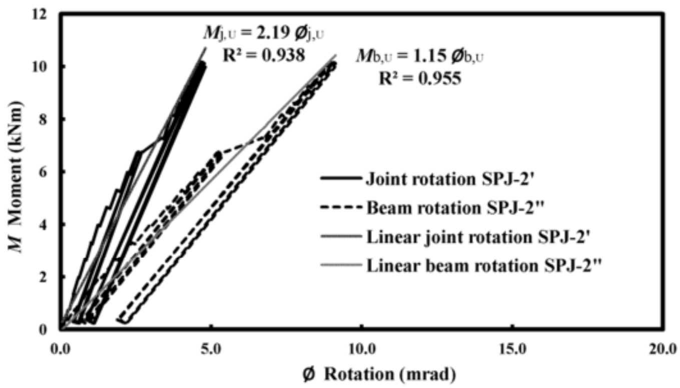

Figure 19. Cyclic M-ϕ curves up to the design ULS moment for SPJ-2.

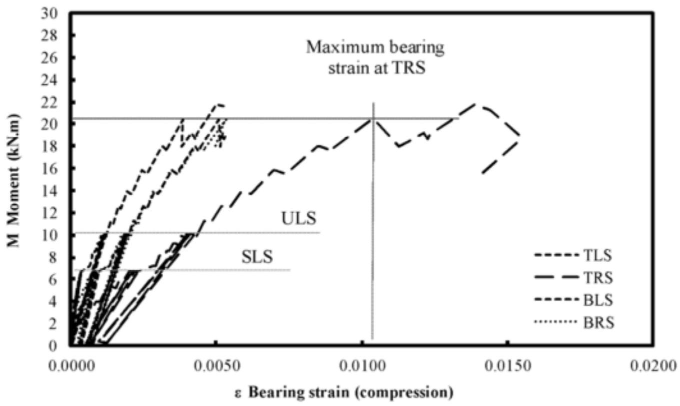

Figure 20. M-ε curves for SPJ-2.

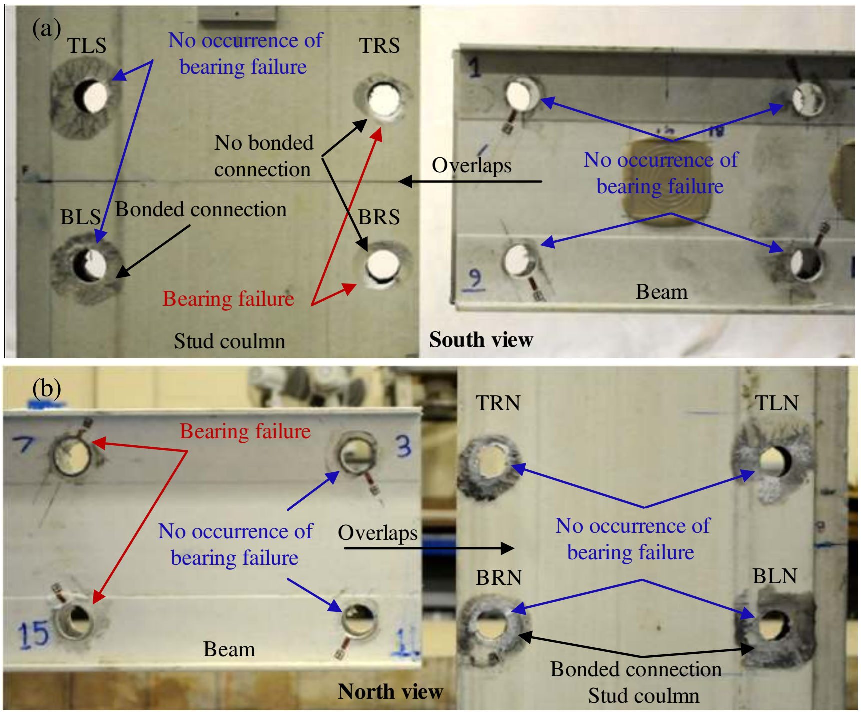

Figure 21. SPJ-2 debonding and bearing failures: (a) South view; (b) North view.